



OPEN

Phytoassisted synthesis of CuO and Ag–CuO nanocomposite, characterization, chemical sensing of ammonia, degradation of methylene blue

Muhammad Farooq¹, Shaukat Shujah¹✉, Kamran Tahir², Syed Tasleem Hussain¹, Afaq Ullah Khan³✉, Zainab M. Almarhoon⁴, Khulood Fahad Alabbosh⁵, Abdulaziz A. Alanazi⁶, Talal M. Althagafi⁷ & Magdi E. A. Zaki⁸✉

The elimination of hazardous industrial pollutants from aqueous solutions is an emerging area of scientific research and a worldwide problem. An efficient catalyst, Ag–CuO was synthesized for the degradation of methylene blue, the chemical sensing of ammonia. A simple novel synthetic method was reported in which new plant material *Capparis decidua* was used for the reduction and stabilization of the synthesized nanocatalyst. A Varying amount of Ag was doped into CuO to optimize the best catalyst that met the required objectives. Through this, the Ag–CuO nanocomposite was characterized by XRD, SEM, HR-TEM, EDX, and FTIR techniques. The mechanism of increased catalytic activity with Ag doping involves the formation of charge sink and suppression of drop back probability of charge from conduction to valance band. Herein, 2.7 mol % Ag–CuO exhibited better catalytic activities and it was used through subsequent catalytic experiments. The experimental conditions such as pH, catalyst dose, analyte initial concentration, and contact time were optimized. The as-synthesized nanocomposite demonstrates an excellent degradation efficacy of MB which is 97% at pH 9. More interestingly, the as-synthesized catalyst was successfully applied for the chemical sensing of ammonia even at very low concentrations. The lower limit of detection (LLOD) also called analytic sensitivity was calculated for ammonia sensing and found to be 1.37 ppm.

Water pollution is a worldwide problem faced both by developed and developing countries. In urban areas water is polluted by heavy industrialization while in rural areas it is mostly due to land erosion and mining¹. Industrial water is saturated with both organic pollutants such as dyes like methylene blue, malachite green, methyl orange, etc. and inorganic pollutants such as heavy metal ions like copper, nickel, chromium, arsenic, lead, etc^{2–8}. Water polluted with organic dyes and heavy metals is a serious threat to both land and water systems^{6–8}. Release of these specific pollutants into environment causes the damage to mammalian cells, burning of the eyes, lungs irritation, vomiting, nausea, liver tumors, etc.^{9–12}. Therefore, water require proper treatment and removal of these organic dyes and heavy metals before its discharge to the ecosystem. Conventional methods include membrane separation, electrolytic process, liquid–liquid extraction, ion exchange, and precipitation as carbonates, sulfates, or hydroxides^{13–16}. However, each method has its own advantages and disadvantages depending on its operational cost, working time, ease of experimental setup, chemicals, regeneration, and other overhead expenses^{17–21}. Some

¹Department of Chemistry, Kohat University of Science and Technology, Kohat 26000, Pakistan. ²Institute of Chemical Sciences, Gomal University, D. I. Khan, KP, Pakistan. ³School of Chemistry and Chemical Engineering, Jiangsu University, 301 Xuefu Road, Zhenjiang 212013, China. ⁴Chemistry Department, College of Science, King Saud University, P. O. Box 2455, Riyadh 11451, Saudi Arabia. ⁵Department of Biology, College of Science, University of Hail, Hail 2440, Saudi Arabia. ⁶Department of Chemistry, College of Science and Humanities in Al-Kharj, Prince Sattam Bin Abdulaziz University, Al-Kharj 11942, Saudi Arabia. ⁷Department of Physics, College of Science, Taif University, Taif 21944, Saudi Arabia. ⁸Department of Chemistry, College of Science, Imam Mohammad Ibn Saud Islamic University, Riyadh 11623, Saudi Arabia. ✉email: shaukat.shujah@yahoo.com; afaqchemist@gmail.com; mezaki@imamu.edu.sa

of the most serious disadvantages that make it unacceptable is incomplete removal, high operational energy, and production of toxic sludge that requires disposal²². So, the attention of the researcher is reverting towards adsorption which is economical, speedy, high removal efficiency, simple experimental setup, and applicable at low and high concentration levels^{22,23}. Activated carbon is the most common adsorbent used for the removal of both organic and inorganic stuff. However, its high operational cost and lengthy regeneration procedure have limited its use^{24,25}. So the use of low-cost agricultural waste such as rice husk, plant leaf powder, etc. is becoming the new trend. However low surface area, low adsorption capacity and prolonged removal time of this biosorbent are unavoidable drawbacks that necessitate further search for adsorbent which is economical, sensitive, nontoxic, and can remove adsorbent in low concentration as well^{26,27}.

Various industries use different synthetic and organic dyes for colouring their products. Methylene blue which is also called basic blue-8 is a cationic dye. Its trade names are Urelene blue, Provay blue, Prove blue. It is a heterocyclic organic compound which is frequently used in textile, cosmetics, paper and pharmaceutical industries and biological staining. As medicine this dye can also be used for the treatment of methemoglobinemia but this chemical could not be recommended as medicine because it has very hazardous effects on living things. On inhalation and ingestion this dye can cause permanent injuries in human and in other animals. Methylene blue can cause headache, vomiting, shortness of breath, nausea, diarrhea, high blood pressure, site necrosis (SC), eyes blurring effects and abdominal pain in human beings. Among various modern methods, photocatalytic degradation is a unique method for the cationic dyes elimination process^{28–30}. Photodegradation is a chemical oxidation reaction catalyzed by nanoparticles that can degrade stable organic dyes like methylene blue. Amongst them, ZnO is a well-known photocatalyst that has been explored deeply for its catalytic and adsorption potential but CuO is less common, having all the catalytic properties found in typical metal oxide nanoparticles^{31–33}. CuO is a p-type semiconducting material having a bulk band gap of 1.2 eV which makes it applicable in solar systems, battery anodes, nanofluids, superconducting materials, gas sensors, transistors, magnetic storage devices, lithium-ion batteries, ceramic resistors, IR filters and recently in formation of solid-fuel for rocket vehicles³⁴. All these applications can be dramatically enhanced by doping of transition and non-transition metals which improve their electrical properties by changing the band gap. Mohamed Basith et al. have doped Ni and Fe and observed that band gap width increases up to 4.3 eV^{35,36}. Doping of Ag metal can modify the catalytic and semiconducting properties even better due to its versatile metallic nature. Currently, only a few articles are presents that show the doping of Ag to CuO. In this context Jichun Huang et al. have investigated that Ag doping to CuO can enhance the electrical conductivity of Ag covered CuO nanosheet arrays³⁷. Hooch Anting et al. studied the successful doping of Ag to CuO and applied it for hydrogen sensing³⁸. Nasrin Ghasemi et al. examined the improvement in antibacterial properties by comparing CuO and Ag doped CuO³⁹. Jianbo Yang et al. synthesized Ag–CuO composite nanosheets and investigated the improvement in photocatalytic properties by degrading methyl orange⁴⁰.

Ammonia is one of the toxic chemical species that is readily soluble in water producing ammonium ion. In addition to other uses like paper, plastic, textiles, explosives, pesticides, refrigeration, cleaning products, and yes about 90% of ammonia is used in the fertilizer industry⁴¹. In air, its amount as low as 5 ppm can be recognized by odor. Therefore, the risk of ammonia toxicology to animals is higher as compared to other gases. The adverse effect of ammonia includes irritation of the eyes, nasal, throat, and chest, cough, edema of the throat, shock, restlessness, cyanosis etc.⁴². One of the unique properties of nanoparticles is its successful application in chemical sensing for the presence of various pollutant such as CO, SO₂, NO, N₂O, NO₂ etc. in wastewater^{43,44}. Metal oxide-based chemical sensors are extensively used due to its low cost, easy operation, nontoxic and stability. However great deal of research is in progress to improve its sensitivity, selectivity, and response time^{45,46}. Compare to other metal oxide, ZnO has been extensively used as a chemical sensor. For example, Ahmed et. al. used it for the detection of O₂ gas⁴⁷, Tan et al. for the detection of CO⁴⁸, Ismail et. al. the for detection of N₂H₄⁴⁹, Ganbavle et. al. for detection of NO₂⁵⁰, Leidinger et. al. for detection of volatile organic compounds (VOCs) etc.⁵¹. Some other metal oxides like SrO, TiO₂, Al₂O₃, WO₃, SnO₂, RuO₂ were also reported as chemical sensors^{52,53}. However, very limited work has been published on the chemical sensitivity of CuO. Doping of Ag to CuO can bring even better results due to improvement in electrical properties.

Biological methods also called green methods are ecofriendly, economical single step process that generates a nontoxic product that can be handled easily. In biological methods phytochemicals present in plant extract are used for reduction and stabilization⁵⁴. A. Tresa Babu et al. synthesized Ag-doped CuO in the presence of *Sida rhombifolia* leaf extract and explored its catalytic properties by degradation of stable aromatic dyes⁵⁵. Maruthupanday et. al. prepared CuO nanoparticles using *Camellia japonica* plant extract as a reducing agent and successfully applied it for the optical sensing of various metal ions⁵⁶. Plants encompass diverse secondary metabolites, including alkaloids, flavonoids, saponins, and steroids, which serve crucial functions as both reducing and stabilizing agents during the synthesis of nanoparticles. Flavonoids and saponins have been documented as effective capping agents in regulating the rate of nanostructure formation, mitigating agglomeration tendencies^{57–61}.

In the present article, we have reported the synthesis of Ag-doped CuO (Ag–CuO) in the presence of *Capparis decidua* plant extract to reduce the metal ion and stabilize the product. Many scientific reports show synthesis of Ag–CuO, however most of them adopt chemical synthesis route which have serious impacts on environment. Some synthetic method also followed use of phytochemical present in plant extract, however no work has been published on this reducing phytochemical rich plant, *C. decidua* plant. Additionally, in reported work, the nanocomposites have solid compact physical state due to which they have low surface area, hence their catalytic activities are significantly reduced. In present work, the preparation method is slightly modified so that Ag–CuO have some porous architecture due to evolution of residual gases during calcination. Due to this porosity surface area and catalytic properties are significantly enhanced as compared with the reported work. Different amount of Ag was doped to optimize the product that is most effective in photocatalytic degradation, chemical sensing, and adsorption process. Furthermore, a numerous characterization technique such as XRD, SEM, EDX, HRTEM,

and FTIR were used to measure particle size, shape and bond formation in CuO nanoparticles. Photocatalytic properties of Ag–CuO were examined by degrading methylene blue dye. The as synthesized nanomaterial was applied for the chemical sensing of ammonia in an aqueous solution.

Experimental

Chemicals and materials

The branches of the *C. decidua* plant were collected from the hilly part of Kohat University Pakistan. All the chemicals such as hydrochloric acid, nitric acid, copper sulfate, copper nitrate, lead chloride, lead acetate, ammonium hydroxide, sodium hydroxide, and methylene blue were obtained from Sigma Aldrich Pakistan and used directly without further treatment. A Stock solution of Pb(II) ion was prepared by dissolving a calculated amount of salt in deionized water. A fresh solution of methylene blue and ammonia was prepared in deionized water at the time of use. All the glassware was purchased from Sigma Aldrich Pakistan. The glassware was washed and preheated every time before use.

Synthesis of nanomaterial

Preparation of plant extract

The plant material has complied with the approval of the Department of Botany, Kohat University of Science and Technology, Pakistan, with national, and international guidelines and legislation. The branches of the wild *C. decidua* plant were collected from the suburbs of Lakki Marwat, Pakistan. It was washed with tap water many times and then rinsed with deionized water and soaked at room temperature. Shaded dried branches of the *C. decidua* plant were powdered and 5 g of it was stirred with 100 mL of deionized water. After 2 h of stirring at 60 °C it was filtered and the filtrate was kept in cold storage for further use.

Synthesis of CuO

Calculated amount of copper sulphate was dissolved in 50 mL deionized water and stirred for 20 min. Specific amount of plant extract (20 mL) was added drop wise with constant stirring at 60 °C. After 2 h of stirring the pH was adjusted at 10 with freshly prepared ammonia solution and again stirred for 2 h. Solution was kept in teflon autoclave for 5 h. After that it was filtered and the black mass obtained was dried in oven at 100 °C. It was placed for about 3 h in furnace at 400 °C for calcination. The calcined CuO was grinded and stored in plastic vials.

Synthesis of CuO

Calculated amount of silver nitrate was dissolved in 50 mL deionized water and stirred for about 10 min. 20 mL of plant extract was added drop wise with constant stirring and temperature was maintained at 60 °C. During this procedure pH drops significantly which is adjusted at 9 by adding freshly prepared ammonia solution and again stirred for 2 h. Highly basic pH must be avoided to restrict formation of Oxides and hydroxides. The colour of solution changed to yellow then it was kept in teflon autoclave for 5 h. After that it was filtered and the grey mass obtained was dried in oven at 120 °C. It was grinded and stored in plastic vials.

Synthesis of Ag–CuO

1 g of calcined CuO was added to 20 mL deionized water and sonicated for 10 min. 50 mL of deionized water was added and stirred for 30 min. To this solution 0.02, 0.04, 0.06, 0.08 and 0.1 g of AgNO₃ was added to prepare 0.92%, 1.8%, 2.7%, 3.6% and 4.4% Ag–CuO solution respectively. The percentage of Ag doping was calculated using Eq. (1). Plant extract was added and the solution was continuously stirred. pH was adjusted at 10–11 by adding freshly prepared ammonia solution and stirred for further 2 h. After that it was filtered, dried in oven and the dried mass was Ag–CuO.

$$\% \text{ mol of Ag} = \frac{n \text{ of AgNO}_3}{n \text{ of AgNO}_3 + n \text{ of CuO}} \times 100 \quad (1)$$

where n is number of moles.

Characterization

Synthesized CuO and Ag–CuO were characterized through different techniques. XRD spectra were obtained in the range of 20°–80° to check the crystallinity of the synthesized nanomaterials. Average particle size was calculated using the Scherrer equation. SEM images were obtained to find information about surface morphology, porosity, and surface element distribution. HR-TEM images were studied to obtain crystallite shape, size, and distribution of Ag particles into CuO lattices. EDX peaks were analyzed to check the purity and presence of constituent elements in the nanomaterials. FT-IR spectra was obtained to confirm the formation of metal–oxygen bond and functional groups presents in plant extract and synthesized nanomaterials.

Degradation of MB

The photocatalytic potential of the CuO and Ag–CuO were investigated by degradation of methylene blue (MB). Experimentally, solutions of MB with different concentrations were prepared. The specific amount of the synthesized photocatalyst with different Ag doping, was added and stirred in the batch-type reactor under UV visible light illumination till the equilibrium. A bulb ($\lambda \geq 420$ nm, HPL-N, 125 W, Philips, China) was used to supply visible light irradiation. 5 mL of the mixture was taken out and centrifuged. It was filtered and the dye remaining concentration in the filtrate was determined by checking the absorbance spectrophotometrically. MB has an absorbance band in the visible region at 665 nm. The blue shift in the peak with time confirm the

degradation and removal of MB by the photocatalyst. The effect of various parameters such as Ag doping, pH, catalyst amount, contact time, and dye initial concentration were studied to optimize the experimental condition for maximum removal. The percent degradation of MB was calculated by Eq. (2).

$$\% \text{ Removal} = \frac{C_o - C_e}{C_o} \times 100 \quad (2)$$

where (C_o) is the initial while (C_e) the is final concentration of the analyte.

Chemical sensing of ammonia

Chemical sensing capabilities of 2.7 mol % Ag–CuO were explored against ammonia solution. Experimentally ammonia solutions of 0, 5, 10, 20, 30, and 40 ppm were prepared. 2 mL of the solution was taken and a specific amount of the catalyst was mixed with it. To check the sensing potential its absorbance was measured by UV visible spectrophotometer.

Results and discussion

Characterization

XRD results

The XRD spectra of CuO and 2.7 mol % Ag–CuO are presented in Fig. 1. XRD spectra of pure CuO consist of diffraction peaks at 2θ range of 32.64, 35.74, 38.97, 48.84, 53.32, 58.54, 61.42 and 66.73 represents the planes with indices (110), (111), (200), (−202), (020), (202), (−113) and (022) respectively. The presence of these sharp peaks confirms the monoclinic crystalline structure of CuO. XRD pattern of Ag–CuO shows additional peaks in the region of $2\theta = 38.87$ and 44.63 which represents (1 1 1) and (2 0 0) planes of Ag. The presence of these additional peaks confirms successful doping of Ag to CuO. The particle size was calculated using Debye Scherrer Eq. (4). Average crystallite size was found to be 21.46 and 18.32 nm for CuO and Ag respectively, which also concede with SEM and TEM results.

$$D = \frac{k\lambda}{\beta \cos\theta} \quad (4)$$

here (D) represents nanoparticle size, ($k=0.9$) is constant, (λ) is the Cu K α radiation wavelength, (β) is the peak width measured at half maximum intensity and (θ) is the peak position at 2θ scale.

SEM results

Surface morphologies and particle shapes are deduced from SEM images as shown in Fig. 2a for CuO and Fig. 2b for 2.7 mol % Ag–CuO. Figure 2a clearly shows that CuO possesses spherical and rod-shaped particles. On doping Ag to CuO surface shape is modified to a sponge-like porous architecture that possesses greater surface area as shown in Fig. 2b. Doping may increase the inter-particle distance which creates micropores that result in enhancement of catalytic properties. The evolution of exhaust gases at high temperatures may also be one of the reasons of pores creation.

EDX results

The purity of the sample and the resultant elemental composition of the synthesized, Ag–CuO were checked using EDX spectra as represented by Fig. 2c. EDX spectra of Ag–CuO consist of peaks that are representative of only Cu, O, and Ag. No additional peaks other than the expected ones were observed which confirm the purity of the nanomaterials. Presence of Ag peak also confirm the successful doping to the CuO lattices.

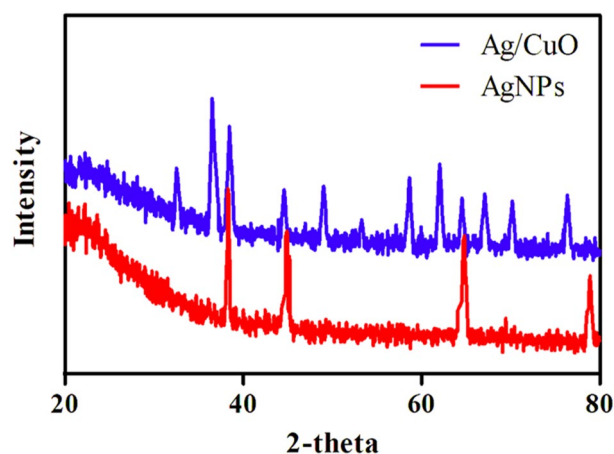


Figure 1. XRD diffractogram of Ag–CuO and Ag nanoparticles.

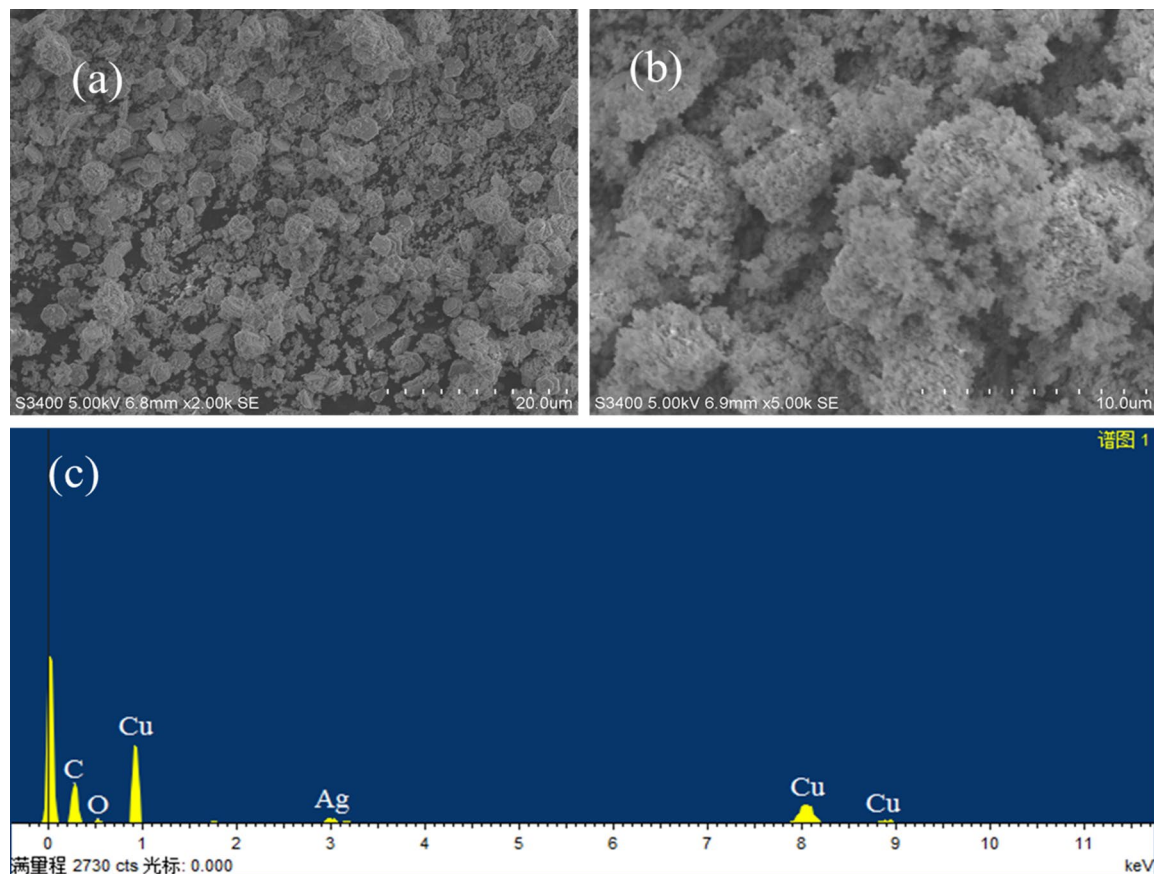


Figure 2. SEM image of (a) CuO (b) Ag-CuO and (c) EDX of Ag-CuO.

TEM results

Morphologies of crystalline nanomaterials and the crystallite size were confirmed by evaluating HRTEM metaphors of CuO and Ag-CuO as shown in Fig. 3a,b respectively. HRTEM images clarify that Ag is uniformly located on the planes of CuO. Lattice fringes with a spacing of 2.84 Å were manifested at a higher magnification level which illustrates the (111) plane of Ag. The average crystallite size lies in the range of 21 nm as manifested by HRTEM is also in accordance with XRD results. Both HRTEM and SEM images show porous sponge like morphologies for Ag-CuO.

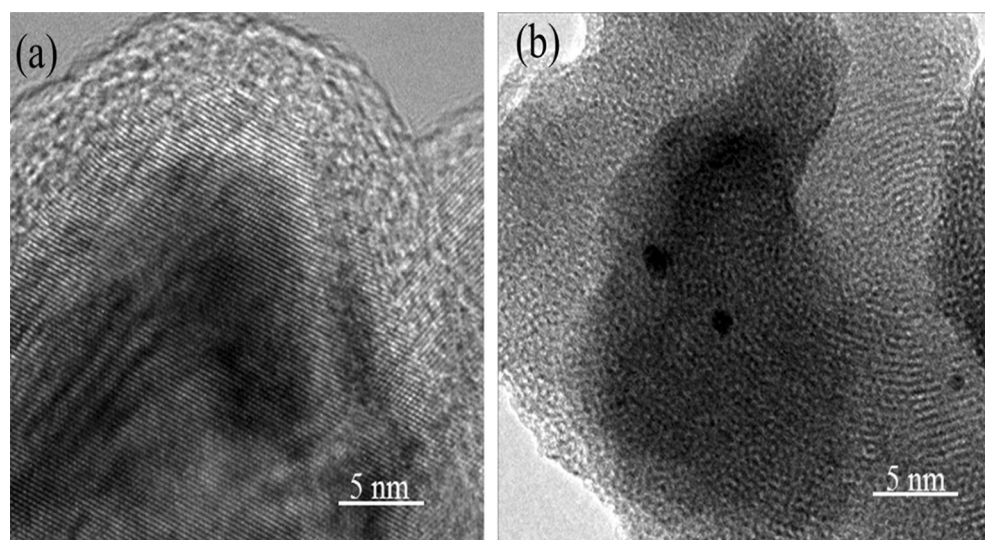


Figure 3. HRTEM image of (a) CuO (b) Ag-CuO.

FTIR results

Various functional groups present in the phytochemicals of plant extract that are necessary for reduction and stabilization were confirmed by FTIR spectra of plant extract as given in Fig. 4a. Additionally, the formation of copper-oxygen bonds is best illustrated by FTIR studies. Broad bands at 3308 cm^{-1} are allotted to hydroxyl groups from plant sources and water. The band at 1623 cm^{-1} also manifests the presence of a hydroxyl group. The bands due to bending and stretching vibrations of the C–H bond are present in the region of 1040 and 2920 cm^{-1} . The absence of a hydroxyl group in the spectra of CuO and the appearance of new bands in the fingerprint region confirm the formation of a copper-oxygen bond, as displayed in Fig. 4b. Metal–oxygen (Cu–O) bond formation is shown by a band at 522 cm^{-1} . C–O bond stretching modes give bands at 1116 cm^{-1} and 1432 cm^{-1} as depicted in CuO spectra Fig. 4b.

Degradation of methylene blue

Effect of Ag doping concentration

To select the photocatalyst with the best activity, the degradation potential of CuO and 0.92, 1.8, 2.7, 3.6, and 4.4 mol% Ag–CuO were examined against methylene blue (MB). 40 ppm solution of MB was taken in batch type reactor and each time a fresh amount (0.4 g/L) of photocatalyst was added under visible irradiation results are depicted by its UV spectra in Fig. 5. In particular, 2.7 mol% Ag–CuO was found best photocatalyst as its activity extends up to 97% as shown in Fig. 6a. Further doping up to 4.4% has a negative effect on photocatalytic activity. Ag doping to CuO enlarges the band gap between the valance and conduction band so the dropback probability of photo-excited electron decreases as Ag is a good sink for a negative charge. Consequently, Ag doping stops the recombination of conduction electrons and positive holes in the valance band which are primary elements responsible for the degradation mechanism⁶². Additionally, doping replaces Cu^{2+} ion with Ag^{1+} ion in the crystal lattice of CuO so due to charge difference oxygen vacancy is created that promotes the photocatalytic activity⁶³. When Ag concentration exceeds its upper limits it agglomerates on the surface and creates a recombination center which demolishes the degradation potential⁶⁴. The upper limit of Ag doping concentration with the best activity is not fixed and it may vary for different metal oxides. Method of preparation of the photocatalyst also affects Ag doping concentration⁶⁵.

The Band gap energy of the said nanomaterials were also examined as shown in Fig. 5B. The band gap energies of Ag, CuO and Ag/CuO were 2.8, 2.5 and 1.7 eV, respectively. The smaller band gap energy of Ag/CuO may be due to their synergistic effect.

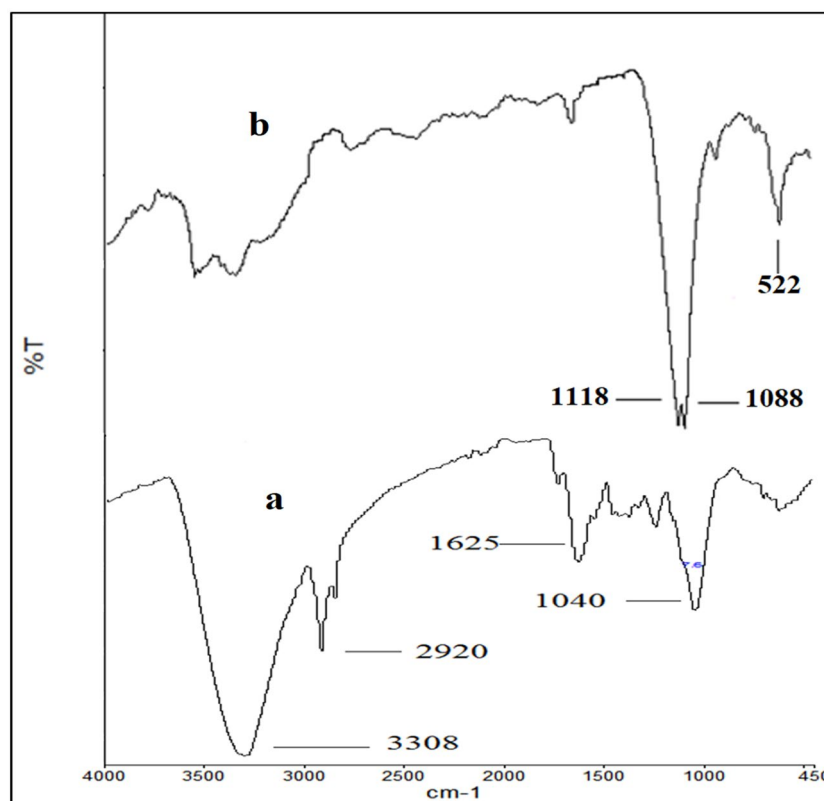


Figure 4. FTIR spectra of (a) Plant extract (b) Ag–CuO.

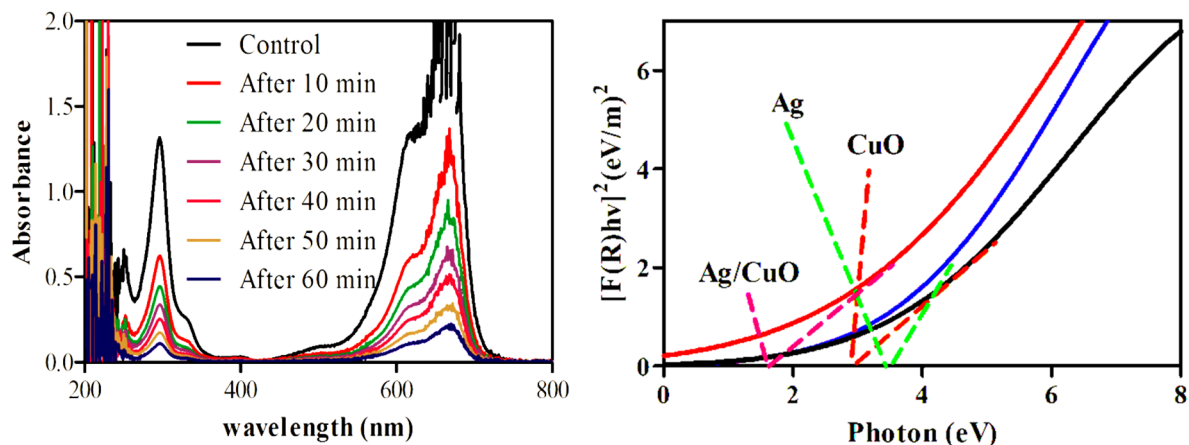


Figure 5. (A) UV/Visible spectra of degradation of methylene blue by Ag–CuO, (B) Band gap energies comparison of Ag, CuO, Ag/CuO.

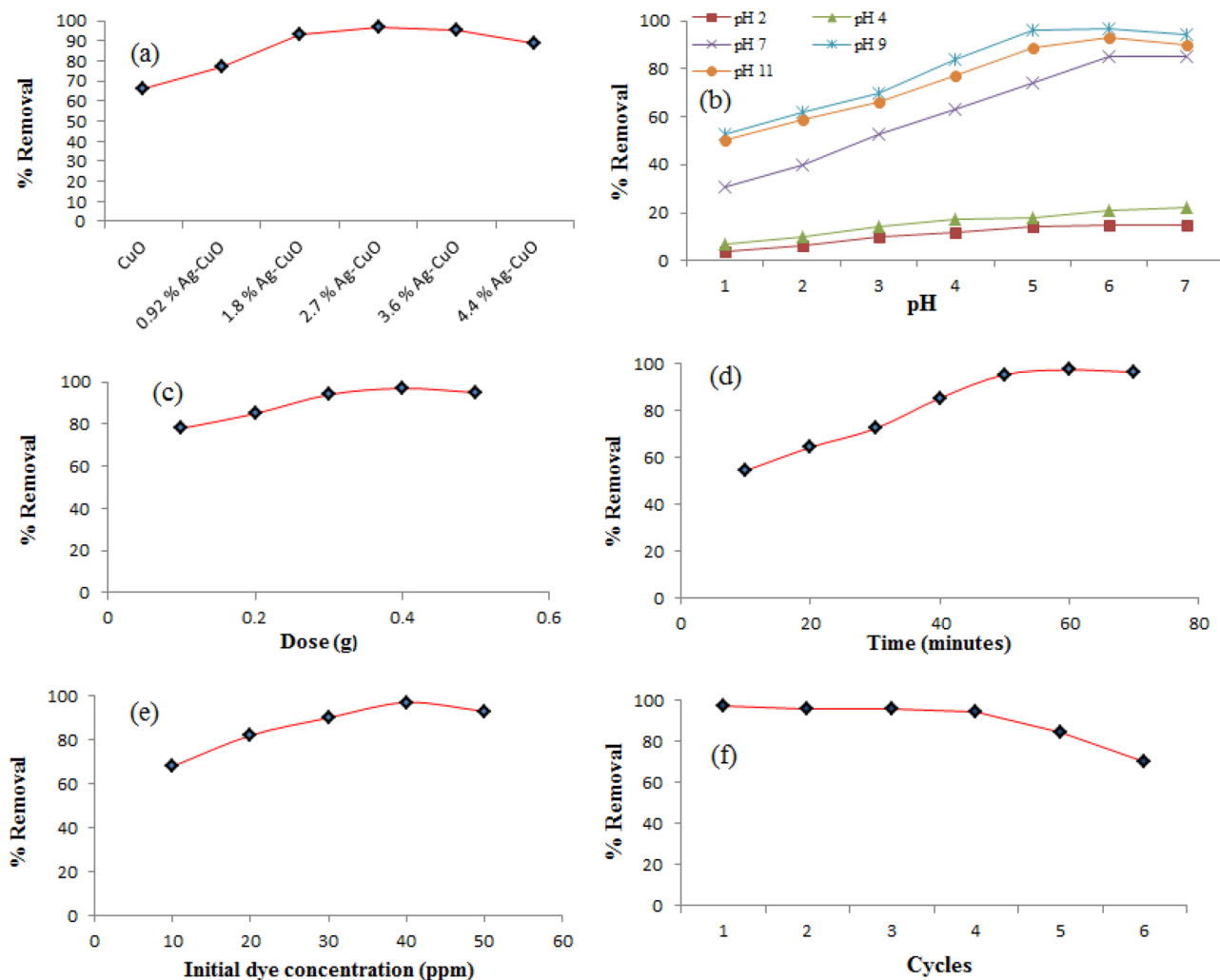


Figure 6. (a) Effect of Ag doping, (b) pH (c) illumination time (d) catalyst loading and (e) dye initial concentration (f) Recyclability study.

Effect of pH

Adsorbent surface chemical nature is greatly affected by the pH of the medium. The effect of pH was examined in the range of 2–11 on 40 ppm MB solution using 0.4 g of 2.7 mol % Ag–CuO under visible light irradiation at room temperature. Maximum efficiency was observed at pH 9 as shown in Fig. 6b. Generally, pH affects the formation of acid–base equilibrium on the surface of the catalyst during adsorption⁶⁶. The pH of medium reflects the surface charge and so the concentration of H^{1+} and OH^{1-} ions. The surface charge of the material is adjusted by pH change such that it attracts opposite charge species due to electrostatic interactions for maximum removal. As MB is a cationic dye with a positive charge and the catalyst surface becomes negatively charged in the basic medium adsorbate–adsorbent interactions increase and so does the degradation⁶⁷.

Effect of catalyst dose

The effect of catalyst dose was studied in the range of 0.1–0.5 using 2.7 mol % Ag–CuO and results are displayed in Fig. 6c. Results show that degradation efficiency increases with an increase in catalyst dose and reaches up to 97% at 0.4 g of catalyst and then decreases. Adsorption is a surface phenomenon that increases with the increase in surface area and amount of the catalyst. As the catalytic amount increases the number of reactive species like photo-excited electrons and oxygen free radicals in the conduction band while positive holes and hydroxyl free radicals in valance band also increases. Combine effect of these two factors results in enhancement of photodegradation ability⁶⁸. Catalytic loading beyond its ideal value results in surface area reduction due to the agglomeration of particles. Also at higher catalytic doses, the solution becomes concentrated, turbid, and opaque so it scatters light, and thus the penetration of visible light irradiation through the solution body is prohibited to reduce photocatalytic degradation⁶⁹.

Effect of contact time

The effect of contact time was examined in the range of 10–80 min for 40 ppm MB solution at pH 9 using 2.7 mol % Ag–CuO as a photocatalyst. Degradation/removal of MB increases directly with an increase in time interval up to the equilibrium. When the equilibrium is established degradation becomes constant with time interval. The equilibrium time for Ag–CuO was observed to be 80 min as shown in Fig. 6d. As time interval increases illumination time increases which excites a greater number of electrons so the number of positive holes and other reactive species also increases which enhances the degradation efficiency⁷⁰.

Effect of initial concentration of dye

Dye initial concentration was varied from 10 to 50 ppm keeping all other parameters constant. It was observed that initially degradation increases with dye concentration then it becomes constant and finally decreases as shown in Fig. 6e. Maximum adsorption was found for 40 ppm initial concentration. When dye initial concentration increases its adsorption increases so the catalyst uncover/bare surface decreases. Therefore, adsorption of OH^{1-} ion decrease on the catalyst, and as a result production of $HO\cdot$ free radical decreases so degradation also decreases⁷¹. A high concentration of dye may also shelter the catalyst surface from visible light irradiation so fewer number of photons strike the surface and the generation of photo-excited electrons decreases. Consequently, the number of reactive species like hydroxyl and oxygen free radical decreases that affect the degradation efficiency⁷².

Photodegradation mechanism of methylene blue

Ag doping to CuO acts as an electron scavenger. Electrons are excited under visible light irradiation from the valance band of CuO to its valance band creating a positive hole in the valance band⁷³. However due wide band gap this process is slow and requires high energy. This problem can be solved efficiently by Ag doping because the fermi level of Ag is lying at a lower level than CuO so a Schottky junction is created that helps electron to jump in multilevel. These photo-excited electrons in the conduction band are captured by Ag^{1+} ion so their dropback probability is minimized. Surface oxygen reacts with electrons in the conduction band in converted to oxygen free radical ($\cdot O_2$). Meanwhile in the valance band positive hole reacts with OH^{1-} from water or base and converts it to hydroxyl free radical ($\cdot OH$). Ag^{1+} in the conduction band also create hydroxyl free radical by reaction with OH^{1-} . These reactive species ($\cdot O_2$ and $\cdot OH$) are unstable, short-lived, strong oxidizing agents that initiate photocatalytic oxidation of tested dye^{74,75}.

Photocatalytic oxidation of MB occurs in many redox reactions, producing many intermediate species that were confirmed by GC-MSD. During degradation blue color of MB fades with time and a hypochromic shift occurs in its UV band at 665 nm as shown in Fig. 5. Actually, MB has many auxochromes in its structure that break during the degradation process⁷⁶. Analysis of degradation products suggests two pathways for the degradation mechanism. One way, which is shown by the red color in Fig. 7, involves the breaking of MB through $-N=C$ and $-S=C$ auxochromes in the middle of two benzene rings. This pathway first generates sulfoxide compounds which break into monosubstituted benzene⁷⁷. Another pathway, as shown by the green color in Fig. 7, consists of N-demethylation of two-sided N, N-dimethyl amine groups in MB⁷⁸. This pathway produce, one heterocyclic three benzene ring product that further breaks down CO_2 and H_2O ⁷⁹.

Recyclability study

One of the important parameters that affect stability, efficiency, and consequently cost is the recyclability of the synthesized adsorbent. 0.1 M HCl was used to regenerate the adsorbent. There was very little difference in the degradation capacity in the first four cycles and then it faded off gradually. The slight decrease in adsorption capacity may be due to the penetration of some MB ions into the pores and thus pore diffusion or intraparticle diffusion occur. The results are displayed graphically in Fig. 6f.

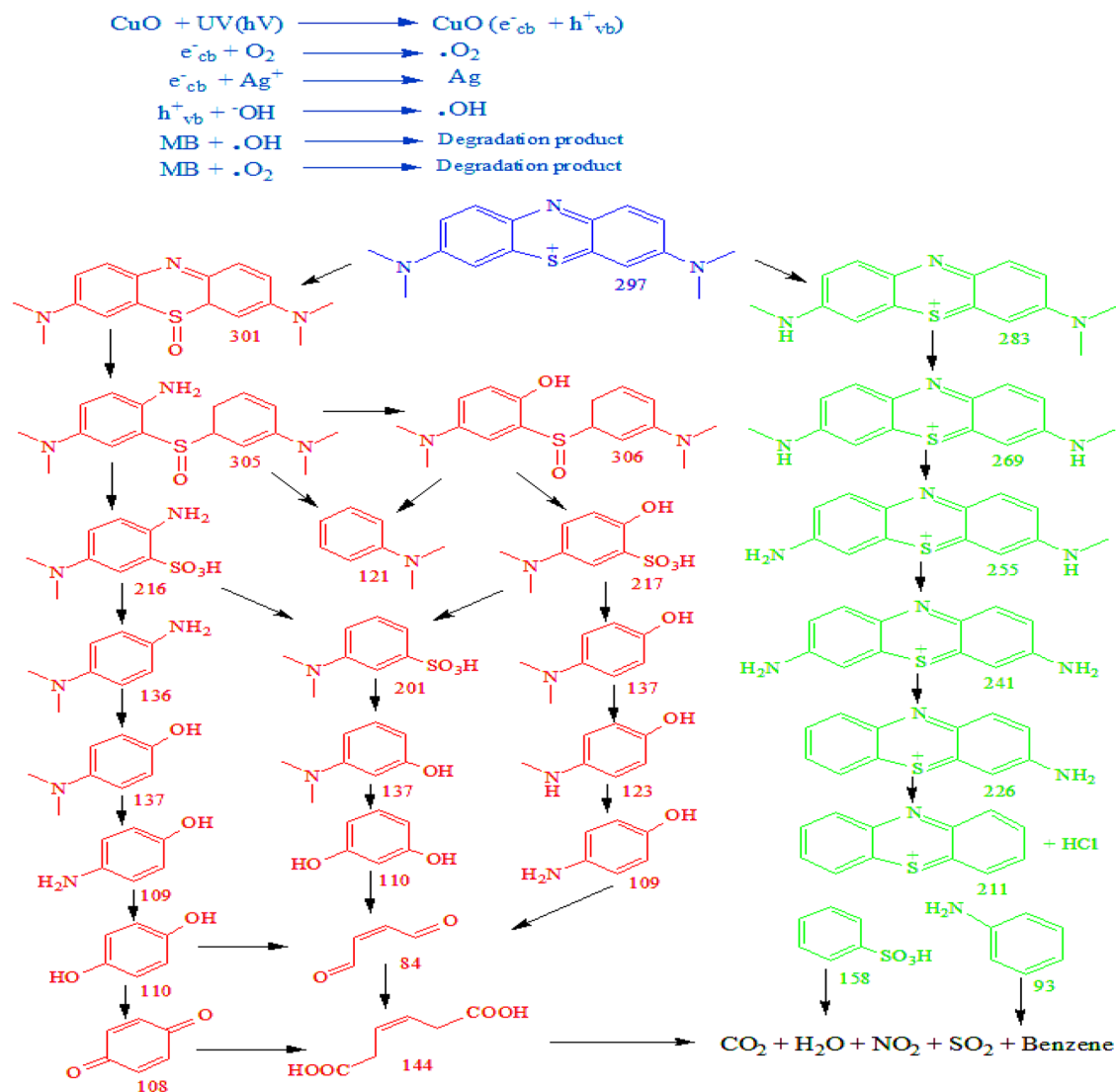


Figure 7. Degradation mechanism of MB.

Comparison of the degradation studies

Table 1 compares the degradation efficacy of the synthetic adsorbent with the usual adsorbents previously described in the literature. It is challenging to select the most effective one because the adsorption capacity depends on the type of adsorbent, the initial concentration of the adsorbate, the preparation method, the cost, etc. The synthesized adsorbent is evaluated against nanomaterials based on CuO, as well as against other metal oxides, and their composites.

Catalyst	pH	Irradiation time (min)	% Degradation	References
Ag-CuO	9	70	92	40
CuO	9	120	63.44	80
Ag-CuO	9	60	94.43	81
CuO	10	50	90.54	82
6Ni-4Cr/TiO	9	90	95.60	83
CuO-TiS ₂	10	180	83.18	84
CuCr ₂ O ₄ /CuO	10	35	90.00	85
Ag-CuO	9	80	97	Present work

Table 1. Comparative studies of photodegradation performance of Ag-CuO nanomaterials.

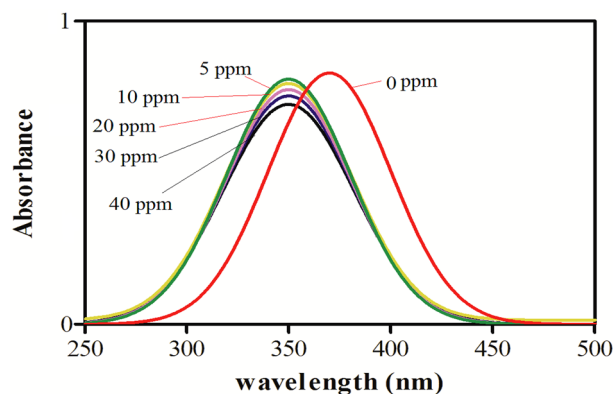


Figure 8. UV/visible spectra of chemical sensing of ammonia by Ag–CuO.

Chemical sensing of ammonia

Ag–CuO was used for chemical sensing of an aqueous solution of ammonia having a concentration in the range of 0–40 ppm and the results are displayed in Fig. 8. As shown in the figure the peak at 350 nm which is due to the surface plasmon resonance (SPRs). In metal nanoparticles, SPRs have an intense and broad absorption band that arises due to the coherent oscillation of electrons in the conduction region near the surface of metal nanoparticles. These SPRs have a critical role in chemical and biological sensing. The blue shift was observed by increasing the ammonia concentration as indicated by a new peak at 310 nm. Changes in the inter-particle distance are usually accountable for this change in SPR shift. So, analysis of absorption spectra is a powerful tool for detecting and calculating the concentration of ammonia solution. The new peak at 310 nm is due to the formation of a coordination complex between ammonia and Ag–CuO nanocomposites. The increasing ammonia concentration from 0 to 40 ppm was monitored by the shift in SPRs position and amplitude in UV–visible spectra⁸⁶. Absorbance data was analyzed to find lower limit of detection (LLOD). It is the smallest amount of analyte that can be detected. LLOD is also called analytic sensitivity. Absorbance data was used to find slope of the graph. From the data standard error intercept (SE intercept) was found. Standard deviation (SD) intercept was calculated by equation ($SD = SE \times \sqrt{N}$) where N is number of sample. From SD, LLOD is calculated by equation ($LLOD = 3 \times SD/\text{slope}$) and found 1.37 ppm.

Conclusion

An efficient nanocatalyst, Ag–CuO was prepared by eco-friendly using *C. decidua* plant material as a natural reducing and stabilizing agent. For this purpose, a different amount of Ag was doped to CuO and based upon degradation of MB, 2.7 mol % Ag–CuO was found more active catalyst as compared to other synthesized Ag–CuO nanocomposite. Here, SEM images exhibit spherical and rod-shaped particles before doping while some sort of softness and formation of sponge-like porous architecture was observed after doping. The HRTEM images showed that Ag is evenly doped on the CuO surface and it gives average crystallite size in the range of 30–90 nm. As a result, the Ag–CuO nanocomposite was found an efficient catalyst as it degrades 97% MB in an aqueous solution. In addition, ammonia was detected chemically even at very low concentrations. The high photocatalytic performance can be attributed to the synergetic coupling of Ag and CuO due to exceptional hollow hierarchical morphology that facilitates the proficient transportation and separation of the photo-generated charges during reaction hence boosting the photocatalytic performance.

Data availability

All data generated or analyzed during this study are included in this published article.

Received: 26 July 2023; Accepted: 4 January 2024

Published online: 18 January 2024

References

1. Raichur, A. M. & Panvekar, V. Removal of As(V) by adsorption onto mixed rare earth oxides. *Sep. Sci. Technol.* **37**, 1095–1108 (2002).
2. Khan, A. U. *et al.* A facile fabrication of silver/copper oxide nanocomposite: An innovative entry in photocatalytic and biomedical materials. *Photodiagn. Photodyn. Ther.* **31**, 101814 (2020).
3. Khan, A. U. *et al.* Biosynthesis of silver capped magnesium oxide nanocomposite using *Olea cuspidata* leaf extract and their photocatalytic, antioxidant and antibacterial activity. *Photodiagn. Photodyn. Ther.* **33**, 102153 (2021).
4. Ngomsik, A.-F. *et al.* Co(II) removal by magnetic alginate beads containing Cyanex 272[®]. *J. Hazard. Mater.* **166**, 1043–1049 (2009).
5. Naiya, T. K., Bhattacharya, A. K. & Das, S. K. Adsorption of Cd(II) and Pb(II) from aqueous solutions on activated alumina. *J. Colloid Interface Sci.* **333**, 14–26 (2009).
6. Yulizar, Y., Abdullah, I., Surya, R. M. & Alifa, N. L. Green synthesis of novel YMnO₃-doped TiO₂ for enhanced visible-light-driven photocatalytic degradation of malachite green. *J. Environ. Manage.* **342**, 118139 (2023).
7. Halomoan, I., Yulizar, Y., Surya, R. M. & Apriandanu, D. O. B. Facile preparation of CuO-Gd₂Ti₂O₇ using *Acmella uliginosa* leaf extract for photocatalytic degradation of malachite green. *Mater. Res. Bull.* **150**, 111726 (2022).

8. Yulizar, Y., Apriandanu, D. O. B. & Marcony Surya, R. Fabrication of novel SnWO₄/ZnO using *Muntingia calabura* L. leaf extract with enhanced photocatalytic methylene blue degradation under visible light irradiation. *Ceram. Int.* **48**, 3564–3577 (2022).
9. Cheng, W. *et al.* Removal of malachite green (MG) from aqueous solutions by native and heat-treated anaerobic granular sludge. *Biochem. Eng. J.* **39**, 538–546 (2008).
10. Khan, S., Cao, Q., Zheng, Y. M., Huang, Y. Z. & Zhu, Y. G. Health risks of heavy metals in contaminated soils and food crops irrigated with wastewater in Beijing, China. *Environ. Pollut.* **152**, 686–692 (2008).
11. Tesfaw, B., Chekol, F., Mehretie, S. & Admassie, S. Adsorption of Pb(II) ions from aqueous solution using lignin from *Hagenia abyssinica*. *Bull. Chem. Soc. Ethiop.* **30**, 473–484 (2016).
12. Khan, A. U. *et al.* A *Tagetes minuta* based eco-benign synthesis of multifunctional Au/MgO nanocomposite with enhanced photocatalytic, antibacterial and DPPH scavenging activities. *Mater. Sci. Eng., C* **126**, 112146 (2021).
13. Hota, G., Kumar, B. R., Ng, W. J. & Ramakrishna, S. Fabrication and characterization of a boehmite nanoparticle impregnated electrospun fiber membrane for removal of metal ions. *J. Mater. Sci.* **43**, 212–217 (2008).
14. Afkhami, A. & Conway, B. E. Investigation of removal of Cr(VI), Mo(VI), W(VI), V(IV), and V(V) oxy-ions from industrial waste-waters by adsorption and electrosorption at high-area carbon cloth. *J. Colloid Interface Sci.* **251**, 248–255 (2002).
15. Afkhami, A., Madrakian, T., Amini, A. & Karimi, Z. Effect of the impregnation of carbon cloth with ethylenediaminetetraacetic acid on its adsorption capacity for the adsorption of several metal ions. *J. Hazardous Mater.* **150**, 408–412 (2008).
16. Wang, J. & Chen, C. Biosorbents for heavy metals removal and their future. *Biotechnol. Adv.* **27**, 195–226 (2009).
17. Pacheco, S., Tapia, J., Medina, M. & Rodriguez, R. Cadmium ions adsorption in simulated wastewater using structured alumina-silica nanoparticles. *J. Non-Crystalline Solids* **352**, 5475–5481 (2006).
18. Apriandanu, D. O. B. & Yulizar, Y. *Tinospora crispa* leaves extract for the simple preparation method of CuO nanoparticles and its characterization. *Nano-Struct. Nano-Objects* **20**, 100401 (2019).
19. Umar, A., Sabrina, V. & Yulizar, Y. Synthesis of ZnO nanoparticles using *Sapindus rarak* DC fruit pericarp extract for rhodamine B photodegradation. *Inorg. Chem. Commun.* **141**, 109593 (2022).
20. Yulizar, Y., Gunlazuardi, J., Apriandanu, D. O. B. & Syahfitri, T. W. W. CuO-modified CoTiO₃ via *Catharanthus roseus* extract: A novel nanocomposite with high photocatalytic activity. *Mater. Lett.* **277**, 128349 (2020).
21. Yulizar, Y., Eprasatya, A., Bagus Apriandanu, D. O. & Yunarti, R. T. Facile synthesis of ZnO/GdCoO₃ nanocomposites, characterization and their photocatalytic activity under visible light illumination. *Vacuum* **183**, 109821 (2021).
22. Aklil, A., Mouflih, M. & Sebti, S. Removal of heavy metal ions from water by using calcined phosphate as a new adsorbent. *J. Hazardous Mater.* **112**, 183–190 (2004).
23. Santos Yabe, M. J. & de Oliveira, E. Heavy metals removal in industrial effluents by sequential adsorbent treatment. *Adv. Environ. Res.* **7**, 263–272 (2003).
24. Heidari, A., Younesi, H. & Mehraban, Z. Removal of Ni(II), Cd(II), and Pb(II) from a ternary aqueous solution by amino functionalized mesoporous and nano mesoporous silica. *Chem. Eng. J.* **153**, 70–79 (2009).
25. Rao, M. M., Ramana, D. K., Seshaiha, K., Wang, M. C. & Chien, S. W. C. Removal of some metal ions by activated carbon prepared from *Phaseolus aureus* hulls. *J. Hazardous Mater.* **166**, 1006–1013 (2009).
26. Jiang, M., Wang, Q., Jin, X. & Chen, Z. Removal of Pb(II) from aqueous solution using modified and unmodified kaolinite clay. *J. Hazardous Mater.* **170**, 332–339 (2009).
27. Munagapati, V. S., Yarramuthi, V., Nadavala, S. K., Alla, S. R. & Abburi, K. Biosorption of Cu(II), Cd(II) and Pb(II) by *Acacia leucocephala* bark powder: Kinetics, equilibrium and thermodynamics. *Chem. Eng. J.* **157**, 357–365 (2010).
28. Türker, A. R. New sorbents for solid-phase extraction for metal enrichment. *CLEAN Soil Air Water.* **35**, 548–557 (2007).
29. Nanoscale iron particles for environmental remediation: An overview|SpringerLink. <https://doi.org/10.1023/A:1025520116015>.
30. Suwarno, A. C., Yulizar, Y., Apriandanu, D. O. B. & Surya, R. M. Biosynthesis of Dy₂O₃ nanoparticles using *Piper Retrofractum* Vahl extract: Optical, structural, morphological, and photocatalytic properties. *J. Mol. Struct.* **1264**, 133123 (2022).
31. Zhang, G., Dong, Y. Y., Li, X. Y., Wei, Y. & Shu, Q. Effects and mechanisms of oxalate on Cd (II) sorption on goethite at different pH and electrolyte concentration. *Plant Nutr. Fertilizer Sci.* **7**, 305–310 (2001).
32. Adsorption of Pb, Cd, Cu, Zn, and Ni to titanium dioxide nanoparticles: effect of particle size, solid concentration, and exhaustion|SpringerLink. <https://doi.org/10.1007/s11356-010-0382-3>.
33. Yulizar, Y., Apriandanu, D. O. B. & Ashna, R. I. La₂CuO₄-decorated ZnO nanoparticles with improved photocatalytic activity for malachite green degradation. *Chem. Phys. Lett.* **755**, 137749 (2020).
34. Martinson, C. A. & Reddy, K. J. Adsorption of arsenic (III) and arsenic (V) by cupric oxide nanoparticles. *J. Colloid Interface Sci.* **336**, 406–411 (2009).
35. Ponnar, M., Thangamani, C., Monisha, P., Gomathi, S. S. & Pushpanathan, K. Influence of Ce doping on CuO nanoparticles synthesized by microwave irradiation method. *Appl. Surface Sci.* **449**, 132–143 (2018).
36. Basith, N. M., Vijaya, J. J., Kennedy, L. J. & Bououdina, M. Structural, optical and room-temperature ferromagnetic properties of Fe-doped CuO nanostructures. *Physica E Low-dimensional Syst. Nanostruct.* **53**, 193–199 (2013).
37. Huang, J., Wu, H., Cao, D. & Wang, G. Influence of Ag doped CuO nanosheet arrays on electrochemical behaviors for supercapacitors. *Electrochimica Acta* **75**, 208–212 (2012).
38. Hooch Antink, W., Choi, Y., Seong, K. & Piao, Y. Simple synthesis of CuO/Ag nanocomposite electrode using precursor ink for non-enzymatic electrochemical hydrogen peroxide sensing. *Sensors Actuators B Chem.* **255**, 1995–2001 (2018).
39. Ghasemi, N., Jamali-Sheini, F. & Zekavati, R. CuO and Ag/CuO nanoparticles: Biosynthesis and antibacterial properties. *Mater. Lett.* **196**, 78–82 (2017).
40. Yang, J. *et al.* Controllable synthesis of Ag–CuO composite nanosheets with enhanced photocatalytic property. *Mater. Lett.* **120**, 16–19 (2014).
41. Timmer, B., Olthuis, W. & van den Berg, A. Ammonia sensors and their applications—A review. *Sensors Actuators B Chem.* **107**, 666–677 (2005).
42. Shao, F., Hernandez-Ramirez, F., Prades, J. D., Morante, J. R. & Lopez, N. Assessment and modeling of NH₃-SnO₂ interactions using individual nanowires. *Procedia Eng.* **47**, 293–297 (2012).
43. Wolfrum, E. J., Meglen, R. M., Peterson, D. & Sluiter, J. Metal oxide sensor arrays for the detection, differentiation, and quantification of volatile organic compounds at sub-parts-per-million concentration levels. *Sensors Actuators B Chem.* **115**, 322–329 (2006).
44. Microfabricated gas sensor systems with sensitive nanocrystalline metal-oxide films|SpringerLink. <https://doi.org/10.1007/s11051-005-9036-7>.
45. Vander Wal, R. L. *et al.* Metal-oxide nanostructure and gas-sensing performance. *Sensors Actuators B Chem.* **138**, 113–119 (2009).
46. Miller, D. R., Akbar, S. A. & Morris, P. A. Nanoscale metal oxide-based heterojunctions for gas sensing: A review. *Sensors Actuators B Chem.* **204**, 250–272 (2014).
47. Ahmed, F., Arshi, N., Anwar, M. S., Danish, R. & Koo, B. H. Mn-doped ZnO nanorod gas sensor for oxygen detection. *Curr. Appl. Phys.* **13**, S64–S68 (2013).
48. Tan, C. H. *et al.* Automated room temperature optical absorbance CO sensor based on In-doped ZnO nanorod. *Sensors Actuators B Chem.* **248**, 140–152 (2017).
49. Ismail, A. A. *et al.* A sensitive and selective amperometric hydrazine sensor based on mesoporous Au/ZnO nanocomposites. *Mater. Design* **109**, 530–538 (2016).

50. Ganbavle, V. V., Inamdar, S. I., Agawane, G. L., Kim, J. H. & Rajpure, K. Y. Synthesis of fast response, highly sensitive and selective Ni:ZnO based NO₂ sensor. *Chem. Eng. J.* **286**, 36–47 (2016).
51. Leidinger, M., Sauerwald, T., Reimringer, W., Ventura, G. & Schütze, A. Selective detection of hazardous VOCs for indoor air quality applications using a virtual gas sensor array. *J. Sensors Sensor Syst.* **3**, 253–263 (2014).
52. Diéguez, A. *et al.* Morphological analysis of nanocrystalline SnO₂ for gas sensor applications. *Sensors Actuators B Chem.* **31**, 1–8 (1996).
53. Li, X., Bai, J., Liu, Q., Li, J. & Zhou, B. WO₃/W nanopores sensor for Chemical Oxygen Demand (COD) determination under visible light. *Sensors* **14**, 10680–10690 (2014).
54. Maulidiya, A., Yulizar, Y., Bakri, R., Apriandanu, D. O. B. & Surya, R. M. Synthesis and characterizations of Ce₂Zr₂O₇-TiO₂ for increased photocatalytic activity toward degradation of methylene blue. *Ceram. Int.* **48**, 29523–29532 (2022).
55. Babu, A. T. & Antony, R. Green synthesis of silver doped nano metal oxides of zinc & copper for antibacterial properties, adsorption, catalytic hydrogenation & photodegradation of aromatics. *J. Environ. Chem. Eng.* **7**, 102840 (2019).
56. Maruthupandy, M. *et al.* Synthesis of metal oxide nanoparticles (CuO and ZnO NPs) via biological template and their optical sensor applications. *Appl. Surface Sci.* **397**, 167–174 (2017).
57. Indriyani, A., Yulizar, Y., Tri Yunarti, R., Oky Bagus Apriandanu, D. & Marcony Surya, R. One-pot green fabrication of BiFeO₃ nanoparticles via *Abelmoschus esculentus* L. leaves extracts for photocatalytic dye degradation. *Appl. Surface Sci.* **563**, 150113 (2021).
58. Marcony Surya, R., Mauliddiyah, S., Bagus Apriandanu, D. O. & Yulizar, Y. SmMnO₃-decorated ZnO in a hexane-water interface for enhancing visible light-driven photocatalytic degradation of malachite green. *Chemosphere* **304**, 135125 (2022).
59. Yulizar, Y., Apriandanu, D. O. B. & Wibowo, A. P. Plant extract mediated synthesis of Au/TiO₂ nanocomposite and its photocatalytic activity under sodium light irradiation. *Composites Commun.* **16**, 50–56 (2019).
60. Ariyanta, H. A., Ivandini, T. A. & Yulizar, Y. Novel NiO nanoparticles via phytosynthesis method: Structural, morphological and optical properties. *J. Mol. Struct.* **1227**, 129543 (2021).
61. Yulizar, Y., Apriandanu, D. O. B. & Al Jabbar, J. L. Facile one-pot preparation of V₂O₅-Fe₂O₃ nanocomposites using *Foeniculum vulgare* extracts and their catalytic property. *Inorg. Chem. Commun.* **123**, 108320 (2021).
62. Xie, W. *et al.* Surface modification of ZnO with Ag improves its photocatalytic efficiency and photostability. *J. Photochem. Photobiol. A Chem.* **216**, 149–155 (2010).
63. Zheng, Y. *et al.* Ag/ZnO heterostructure nanocrystals: Synthesis, characterization, and photocatalysis. *Inorg. Chem.* **46**, 6980–6986 (2007).
64. Ren, C. *et al.* Synthesis of Ag/ZnO nanorods array with enhanced photocatalytic performance. *J. Hazardous Mater.* **182**, 123–129 (2010).
65. Wang, J., Fan, X. M., Zhou, Z. W. & Tian, K. Preparation of Ag nanoparticles coated tetrapod-like ZnO whisker photocatalysts using photoreduction. *Mater. Sci. Eng. B* **176**, 978–983 (2011).
66. Alkaykh, S., Mbarek, A. & Ali-Shattle, E. E. Photocatalytic degradation of methylene blue dye in aqueous solution by MnTiO₃ nanoparticles under sunlight irradiation. *Heliyon* **6**, 4 (2020).
67. Daneshvar, N., Aber, S., Seyed Dorraji, M. S., Khataee, A. R. & Rasoulifard, M. H. Photocatalytic degradation of the insecticide diazinon in the presence of prepared nanocrystalline ZnO powders under irradiation of UV-C light. *Separat. Purif. Technol.* **58**, 91–98 (2007).
68. Hayat, K., Gondal, M. A., Khaled, M. M. & Ahmed, S. Kinetic study of laser-induced photocatalytic degradation of dye (alizarin yellow) from wastewater using nanostructured ZnO. *J. Environ. Sci. Health Part A* **45**, 1413–1420 (2010).
69. Wang, H. *et al.* Comparison of dye degradation efficiency using ZnO powders with various size scales. *J. Hazardous Mater.* **141**, 645–652 (2007).
70. El-Bahy, Z. M., Ismail, A. A. & Mohamed, R. M. Enhancement of titania by doping rare earth for photodegradation of organic dye (Direct Blue). *J. Hazardous Materials* **166**, 138–143 (2009).
71. Photocatalytic degradation of rhodamine B dye using hydrothermally synthesized ZnO|SpringerLink. <https://doi.org/10.1007/BF02914073>.
72. Mengyue, Z., Shifu, C. & Yaowu, T. Photocatalytic degradation of organophosphorus pesticides using thin films of TiO₂. *J. Chem. Technol. Biotechnol.* **64**, 339–344 (1995).
73. Balasubramanian, J., Ponnaiah, S. K., Periakaruppan, P. & Kamaraj, D. Accelerated photodeterioration of class I toxic monocrotophols in the presence of one-pot constructed Ag₃PO₄/polyaniline@g-C₃N₄ nanocomposite: Efficacy in light harvesting. *Environ. Sci. Pollut. Res.* **27**, 2328–2339 (2020).
74. Okumu, J. *et al.* Photochromic silver nanoparticles fabricated by sputter deposition. *J. Appl. Phys.* **97**, (2005).
75. Ponnaiah, S. K., Prakash, P., Arumuganathan, T. & Jeyaprabha, B. Effectual light-harvesting and electron-hole separation for enhanced photocatalytic decontamination of endocrine disruptor using Cu₂O/BiOI nanocomposite. *J. Photochem. Photobiol. A Chem.* **380**, 111860 (2019).
76. Shirafuji, T., Nomura, A., Hayashi, Y., Tanaka, K. & Goto, M. Matrix-assisted laser desorption ionization time-of-flight mass spectrometric analysis of degradation products after treatment of methylene blue aqueous solution with three-dimensionally integrated microsolution plasma. *Japan. J. Appl. Phys.* **55**(1S), 01AH02 (2015).
77. Wang, Q., Tian, S. & Ning, P. Degradation mechanism of methylene blue in a heterogeneous Fenton-like reaction catalyzed by ferrocene. *Ind. Eng. Chem. Res.* **53**, 643–649 (2014).
78. Xia, S., Zhang, L., Pan, G., Qian, P. & Ni, Z. Photocatalytic degradation of methylene blue with a nanocomposite system: Synthesis, photocatalysis and degradation pathways. *Phys. Chem. Chem. Phys.* **17**, 5345–5351 (2015).
79. Luan, J. & Hu, Z. Synthesis, property characterization, and photocatalytic activity of novel visible light-responsive photocatalyst. *Int. J. Photoenergy* **2012**, 1–11 (2012).
80. Riapanitra, A., Riyani, K. & Setyaningtyas, T. Photocatalytic and kinetics study of copper oxide on the degradation of methylene blue dye. in *Soedirman International Conference on Mathematics and Applied Sciences (SICOMAS 2021)* 1–5 (Atlantis Press, 2022).
81. Baste, Y. *et al.* Polyol synthesis of Ag-doped copper oxide nanoparticles as a methylene blue-degrading agent. *Catalysts* **13**, 1143 (2023).
82. Jassim, H. A., Khadhim, A. & Al-Amiery, A. A. Photo catalytic degradation of methylene blue by using CuO nanoparticles. *Int. J. Comput. Appl. Sci* **1**, 1–4 (2016).
83. Shaban, M., Ahmed, A. M., Shehata, N., Betiha, M. A. & Rabie, A. M. Ni-doped and Ni/Cr co-doped TiO₂ nanotubes for enhancement of photocatalytic degradation of methylene blue. *J. Colloid Interface Sci.* **555**, 31–41 (2019).
84. Parvaz, M., Khan, M. B., Azam, A. & Khan, Z. H. Synthesis, characterization, and photocatalytic properties of CuO-TiSi₂ nanocomposite. *Mater. Res. Express* **6**, 125054 (2019).
85. Hariganesh, S. *et al.* Facile large scale synthesis of CuCr₂O₄/CuO nanocomposite using MOF route for photocatalytic degradation of methylene blue and tetracycline under visible light. *Appl. Organometal. Chem.* **34**, e5365 (2020).
86. Peng, S., McMahon, J. M., Schatz, G. C., Gray, S. K. & Sun, Y. Reversing the size-dependence of surface plasmon resonances. *Proc. Natl. Acad. Sci.* **107**, 14530–14534 (2010).

Acknowledgements

This research was supported by the Deanship of Scientific Research, Imam Mohammad Ibn Saud Islamic University (IMSIU), Saudi Arabia.

Author contributions

M.F.: Writing—original draft, Investigation. S.S.: Supervision, Conceptualization, Methodology. K.T.: Writing—review & editing, Validation. S.T.H.: Formal analysis. A.U.K.: Conceptualization, Writing—review & editing. Z.M.A.: Validation, visualization. K.F.A.: Data curation. A.A.A.: Review & editing and software. T.M.A.: Software, Resources. M.E.A.Z.: Funding acquisition, Resources, Supervision.

Competing interests

The authors declare no competing interests.

Additional information

Correspondence and requests for materials should be addressed to S.S., A.U.K. or M.E.A.Z.

Reprints and permissions information is available at www.nature.com/reprints.

Publisher's note Springer Nature remains neutral with regard to jurisdictional claims in published maps and institutional affiliations.



Open Access This article is licensed under a Creative Commons Attribution 4.0 International License, which permits use, sharing, adaptation, distribution and reproduction in any medium or format, as long as you give appropriate credit to the original author(s) and the source, provide a link to the Creative Commons licence, and indicate if changes were made. The images or other third party material in this article are included in the article's Creative Commons licence, unless indicated otherwise in a credit line to the material. If material is not included in the article's Creative Commons licence and your intended use is not permitted by statutory regulation or exceeds the permitted use, you will need to obtain permission directly from the copyright holder. To view a copy of this licence, visit <http://creativecommons.org/licenses/by/4.0/>.

© The Author(s) 2024